# Relativistic convergent close-coupling method calculation of the spin polarization of electrons scattered elastically from zinc and mercury

Christopher J. Bostock,* Dmitry V. Fursa, and Igor Bray
*Australian Research Council Centre for Antimatter-Matter Studies, Curtin University, GPO Box U1987, Perth, Western Australia 6845, Australia*

(Received 14 May 2012; revised manuscript received 5 June 2012; published 25 June 2012)

We present spin-asymmetry parameters (Sherman functions) for elastic electron scattering on zinc and mercury atoms calculated using the relativistic convergent close-coupling method for quasi-two-electron atoms above an inert core. The results for mercury are in excellent agreement with experiment across a wide range of energies. Similarly for zinc, we find excellent agreement between theory and experiment for energies below 9.0 eV. However, at 11.0 eV there is a discrepancy between theory and experiment, most likely due to a resonance excitation of a core electron.

DOI: 10.1103/PhysRevA.85.062707 PACS number(s): 34.80.Bm, 34.80.Dp, 34.80.Nz

## I. INTRODUCTION

Electron scattering from zinc and mercury has received recent attention in the literature due to a discrepancy between theory and experiment for the Zn $P_2$ Stokes parameter of light emitted during spin-polarized electron-impact excitation below the ionization threshold [1,2]. A controversial claim is made by Williams *et al*. [2] that relativistic scattering theories do not account for spin properly during electron scattering on quasi-two-electron targets such as Zn and Hg; the claim is made that a geometric Berry phase is required to augment fundamental scattering theories. In order to contest such a claim we present calculations of the Sherman function for electron scattering on Zn and Hg across a wide range of energies. The relativistic convergent close-coupling (RCCC) method [3,4] is nonperturbative and involves solving a set of relativistic Lippmann-Schwinger equations derived from the Dirac equation. Therefore the spin-orbit interaction is included *ab initio* in a consistent way between all electrons in the electron-target collision system. The unitarity of the RCCC method ensures that the effect of excitation channels is taken into account during the calculation of the Sherman function, which pertains to elastic scattering; the total flux is conserved and therefore opening of excitation channels affects the elastic channel. Relativistic convergent close-coupling results for scattering on other quasi-two-electron targets such as Cd [5,6] demonstrate the effectiveness of the method in comparison to perturbative relativistic distorted-wave methods.

Spin-polarization effects in electron scattering from atoms can be due to electron exchange, spin-orbit interactions, or their interference [7–10]. For the case of elastic electron scattering from a spin-zero target such as the Zn or Hg ground state, the spin-polarization effects arise solely due to the spin-orbit interactions [11]. The exchange effects, while important in determining the magnitude of the cross section at low energies, do not give rise explicitly to any spin polarization in the scattering process. Conversely, even for low-energy electrons incident on a heavy target, the spin-orbit interaction can influence spin-polarization effects in scattering because the electrons will accelerate significantly on approaching close to the nucleus. Thus the study of spin-polarization effects in electron-zinc and electron-mercury scattering provides a sensitive test of the relativistic effects and correct antisymmetrization of the total wave function.

The RCCC results for the Zn Sherman function are compared with the measurements of Bartsch *et al*. [12] and the relativistic distorted-wave calculations of McEachran and Stauffer [13], Szmytkowski and Sienkiewicz [14], and Kumar *et al*. [15]. For the Hg Sherman function, the RCCC results are compared with the measurements of Dummler *et al*. [16], Kaussen *et al*. [17], and Duweke *et al*. [18] and also the following theories: the relativistic distorted-wave calculations of Szmytkowski and Sienkiewicz [14], the generalized density-functional calculations of Fritsche *et al*. [19] and Haberland and Fritsche [20], and *R*-matrix calculations of Bartschat *et al*. [21].

## II. METHOD

The RCCC method is described in detail by Bostock [4] and only a brief overview relevant for the case of *e*-Zn and *e*-Hg scattering will be presented. The Zn atom is modeled as two active valence electrons above a frozen [Ar]$3d^{10}$ Dirac-Fock core. The [Ar]$3d^{10}$ Dirac-Fock core orbitals are obtained using the GRASP package [22]. For the valence electrons, a set of one-electron orbitals is obtained by diagonalization of the $Zn^+$ quasi-one-electron Dirac-Coulomb Hamiltonian in a relativistic (Sturmian) $L$-spinor basis [23]. The set of orbitals contains $4s$–$10s$, $4p_j$–$9p_j$, and $4d_j$–$8d_j$ ($j = l \pm 1/2$) orbitals. Two-electron configuration-interaction calculations are then performed to obtain wave functions for the Zn atom. The choice of two-electron configurations was such that one electron is in $4s$,$4p_{1/2}$, or $4p_{3/2}$ orbitals while the other electron occupies any of the one-electron orbitals allowed by the total angular momentum and parity.

Phenomenological one- and two-electron polarization potentials are used to improve the accuracy of the calculated Zn wave functions [24,25]; these allow us to take into account more accurately the effect of closed inert shells on the active electrons. These depend on the static dipole polarizability of the inert core $\alpha_c$, which is given by the calculations of Ye and Wang [26]. The parameters of these potentials, the static dipole

*c.bostock@curtin.edu.au

 

TABLE I. The RCCC energy levels for Zn compared with experimental levels listed by the National Institute of Standards and Technology (NIST) [28].

| Configuration | Term | $J$ | Parity | RCCC (eV) | Experiment (eV) |
|---|---|---|---|---|---|
| $4s^2$ | $^1S_0$ | 0.0 | 1 | 0.000 | 0.000 |
| $4s4p$ | $^3P^o_0$ | 0.0 | −1 | 4.064 | 4.006 |
| $4s4p$ | $^3P^o_1$ | 1.0 | −1 | 4.091 | 4.030 |
| $4s4p$ | $^3P^o_2$ | 2.0 | −1 | 4.144 | 4.078 |
| $4s4p$ | $^1P^o_1$ | 1.0 | −1 | 5.882 | 5.796 |
| $4s5s$ | $^3S_1$ | 1.0 | 1 | 6.648 | 6.655 |
| $4s5s$ | $^1S_0$ | 0.0 | 1 | 6.698 | 6.917 |
| $4s5p$ | $^3P^o_0$ | 0.0 | −1 | 7.609 | 7.594 |
| $4s5p$ | $^3P^o_1$ | 1.0 | −1 | 7.613 | 7.597 |
| $4s5p$ | $^3P^o_2$ | 2.0 | −1 | 7.620 | 7.604 |
| Ionization limit | | | | 9.396 | 9.394 |

polarizability, the falloff radius $r_c^{\rm pol}$, and $r_c^{\rm diel}$ are adjusted to obtain the best representation of target state energies and optical oscillator strength (OOS). For the $Zn^{2+}$ core we chose $\alpha_c = 2.6$, $r_c^{\rm diel} = 2.1$, and an $l$-dependent $r_c^{\rm pol}$ with values 1.5, 1.5, and 1.6 for $l = 0, 1$, and 2, respectively. The energy levels of the first ten states used in the calculation are listed in Table I and the OOSs for the $(4s4p)\,^3P_1$ and $(4s4p)\,^1P_1$ states are listed in Table II. According to the measurements of Goebel *et al.* [27], the experimental static dipole polarizability of Zn is $38.8a_0^3$. With our target model we obtain a value of $33.1a_0^3$. This slightly lower value is an indication of the imperfection in the $[Ar]3d^{10}$ inert core model as a large part of the static dipole polarizability comes from inner core excitations. In the present work we have chosen the polarization potential parameters to obtain the most accurate energy levels and oscillator strengths possible; this is at the expense of obtaining an accurate value for the static dipole polarizability. Our target model consists of 66 states: 32 bound states and 34 continuum states.

Similarly, the Hg atom is modeled as two active valence electrons above a frozen $[Xe]4f^{14}5d^{10}$ Dirac-Fock core. The $[Xe]4f^{14}5d^{10}$ Dirac-Fock core orbitals are obtained using the GRASP package [22]. For the valence electrons, a set of one-electron orbitals is obtained by diagonalization of the $Hg^+$ quasi-one-electron Dirac-Coulomb Hamiltonian in a relativistic (Sturmian) $L$-spinor basis [23]. The set of orbitals contains $6s$–$17s$, $6p_j$–$17p_j$, $6d_j$–$17d_j$, and $6f_j$–$17f_j$ ($j = l \pm 1/2$) orbitals. Two-electron configuration-interaction calculations are then performed to obtain wave functions for the Hg atom. The choice of two-electron configurations was such that one electron is in $6s$,$6p_{1/2}$, or $6p_{3/2}$ orbitals while the other electron occupies any of the one-electron orbitals allowed by the total angular momentum and parity.

TABLE II. Oscillator strengths of the Zn ground state. Experimental values listed by NIST [28] are also shown.

| | Oscillator strength | |
|---|---|---|
| Transition | RCCC | Expt. |
| $(4s^2)\,^1S_0$–$(4s4p)\,^3P_1$ | 0.00014 | 0.00019 |
| $(4s^2)\,^1S_0$–$(4s4p)\,^1P_1$ | 1.45 | 1.46 |

TABLE III. The RCCC energy levels for Hg compared with experimental levels listed by NIST [28].

| Configuration | Term | $J$ | Parity | RCCC (eV) | Experiment (eV) |
|---|---|---|---|---|---|
| $6s^2$ | $^1S_0$ | 0.0 | 1 | 0.000 | 0.000 |
| $6s6p$ | $^3P^o_0$ | 0.0 | −1 | 4.706 | 4.667 |
| $6s6p$ | $^3P^o_1$ | 1.0 | −1 | 4.926 | 4.887 |
| $6s6p$ | $^3P^o_2$ | 2.0 | −1 | 5.577 | 5.461 |
| $6s6p$ | $^1P^o_1$ | 1.0 | −1 | 6.549 | 6.704 |
| $6s7s$ | $^3S_1$ | 1.0 | 1 | 7.775 | 7.730 |
| $6s7s$ | $^1S_0$ | 0.0 | 1 | 8.000 | 7.926 |
| $6s7p$ | $^3P^o_0$ | 0.0 | −1 | 8.648 | 8.619 |
| $6s7p$ | $^3P^o_1$ | 1.0 | −1 | 8.667 | 8.637 |
| $6s7p$ | $^3P^o_2$ | 2.0 | −1 | 8.763 | 8.829 |
| Ionization limit | | | | 10.447 | 10.438 |

For the $Hg^{2+}$ core phenomenological polarization parameters we chose $\alpha_c = 8.4$, $r_c^{\rm diel} = 2.3$, and $r_c^{\rm pol} = 2.2$. The energy levels of the first ten states used in the calculation are listed in Table III and the OOSs for the $(6s6p)\,^3P_1$ and $(6s6p)\,^1P_1$ states are listed in Table IV. According to the measurements of Miller and Bederson [29] the experimental static dipole polarizability of Hg is $34.4a_0^3$. With our target model we obtain a value of $22.6a_0^3$. Similarly to the Zn atom, this lower value is an indication of the imperfection in the frozen $[Xe]4f^{14}5d^{10}$ inert core model as a large part of the static dipole polarizability comes from inner core excitations. Our target model consists of 58 states: 29 bound states and 29 continuum states.

The generated target states are then used to expand the total wave function of the electron-zinc scattering system and formulate a set of relativistic Lippmann-Schwinger equations for the $T$-matrix elements. In this latter step, the relativistic Lippmann-Schwinger equations for the $T$-matrix elements have the partial wave form

$$T^{\Pi J}_{fi}(k_f\kappa_f, k_i\kappa_i) = V^{\Pi J}_{fi}(k_f\kappa_f, k_i\kappa_i) + \sum_n \sum_\kappa \int\!\!\!\!\!\!- dk \frac{V^{\Pi J}_{fn}(k_f\kappa_f, k\kappa) T^{\Pi J}_{ni}(k\kappa, k_i\kappa_i)}{E - \epsilon^N_n - \epsilon_{k'} + i0}. \quad (1)$$

The notation in Eq. (1), the matrix elements, and the method of solution using a hybrid OpenMP-MPI parallelization suitable for high-performance supercomputing architectures are given in Ref. [4].

The $T$-matrix elements obtained from solution of Eq. (1) are used to determine the scattering amplitudes [4], which in turn are used to calculate the spin-asymmetry parameter $S_A$. For scattering of unpolarized spin-$\frac{1}{2}$ electrons on an unpolarized

TABLE IV. Oscillator strengths of the Hg ground state. Experimental values listed by NIST [28] are also shown.

| | Oscillator strength | |
|---|---|---|
| Transition | RCCC | Expt. |
| $(6s^2)\,^1S_0$–$(6s6p)\,^3P_1$ | 0.038 | 0.024 |
| $(6s^2)\,^1S_0$–$(6s6p)\,^1P_1$ | 1.20 | 1.16 |

target this is given by Scott *et al.* [30],

$$S_A = \frac{-2}{\sigma_u(2J_0+1)}\mathrm{Im}\left\{\sum_{M_1 M_0} f\left(M_1\tfrac{1}{2};M_0-\tfrac{1}{2}\right) \times f^*\left(M_1\tfrac{1}{2};M_0\tfrac{1}{2}\right)\right\}, \quad (2)$$

where Im{} denotes the imaginary part and the cross section $\sigma_u$ is

$$\sigma_u = \frac{1}{2(2J_0+1)}\sum_{M_1 M_0 m_1 m_0}|f(M_1 m_1;M_0 m_0)|^2. \quad (3)$$

The scattering amplitude $f(M_1 m_1; M_0 m_0)$ describes the transition from a target state with total angular momentum $J_0$ and spin projection $M_0$ to a target state with $J_1$ and $M_1$. The initial and final spin projections of the scattered electron are $m_0$ and $m_1$, respectively. For elastic scattering of unpolarized electrons on an unpolarized spin-zero target the $S_A$ parameter is equivalent to the Sherman function [31]. Note that the nonrelativistic convergent close-coupling method has a zero spin-flip amplitude [$f(0\frac{1}{2};0-\frac{1}{2})=0$] due to the absence of spin-orbit coupling in the formalism and therefore Eq. (2) yields identically zero for $S_A$.

## III. RESULTS

The results for the RCCC method calculations of the $S_A$ parameter of Zn are illustrated in Fig. 1. Here the

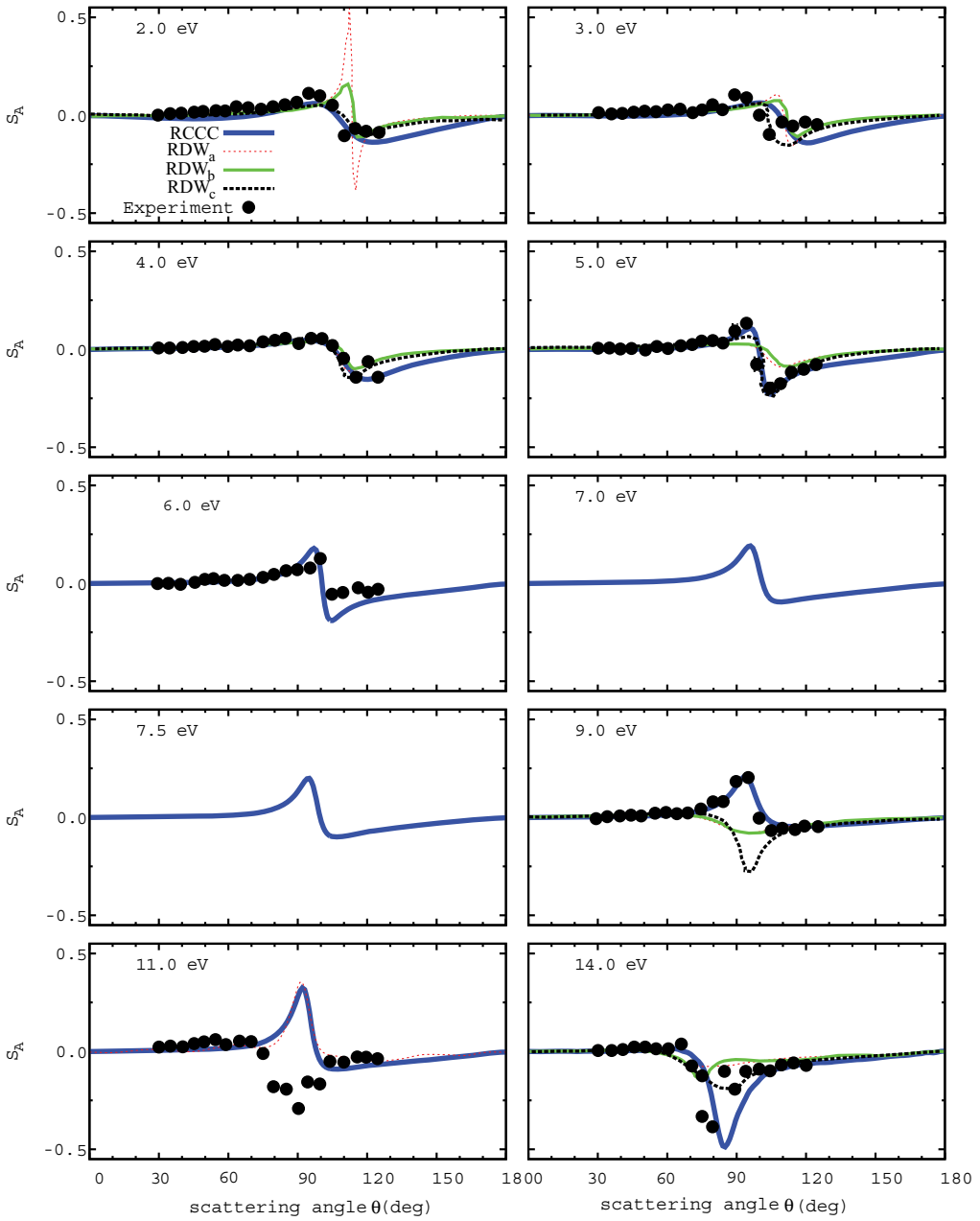


FIG. 1. (Color online) Spin-asymmetry parameter $S_A$ at a range of energies for elastic electron scattering on zinc. Measurements of Bartsch *et al.* [12] are presented. The RCCC calculations are described in the text. Relativistic distorted-wave calculations of McEachran and Stauffer [13], Szmytkowski and Sienkiewicz [14], and Kumar *et al.* [15] are denoted by RDW$_a$, RDW$_b$, and RDW$_c$, respectively.

spin-asymmetry parameter is calculated across a wide range of energies and compared with the measurements of Bartsch *et al*. [12] and the previous relativistic distorted-wave (RDW) calculations of McEachran and Stauffer [13], Szmytkowski and Sienkiewicz [14], and Kumar *et al*. [15]. The RDW calculations utilize first-order perturbative solutions of the Dirac equation for various model potentials. The measurements were taken with an angular resolution of 3.5° and this is incorporated by convolution of the RCCC results. Note in Fig. 1 that there is a significant discrepancy between experiment and previous distorted-wave theories for an electron impact energy of 9.0 eV. The RCCC method, which is both unitary and has a full account of relativistic spin-orbit effects, produces results that are in excellent agreement with experiment at this energy. It has been demonstrated previously in an analysis of spin-resolved electron-sodium scattering that the unitarity of the close-coupling formalism accounts for the influence of excited states on the elastic channel spin asymmetry [32]. At the energies of 2, 3, 4, 5, and 6 eV there is also excellent overall agreement between the RCCC results and experiment. We note that it is in this low-energy region, where cascade effects from high-lying states are absent, that Pravica

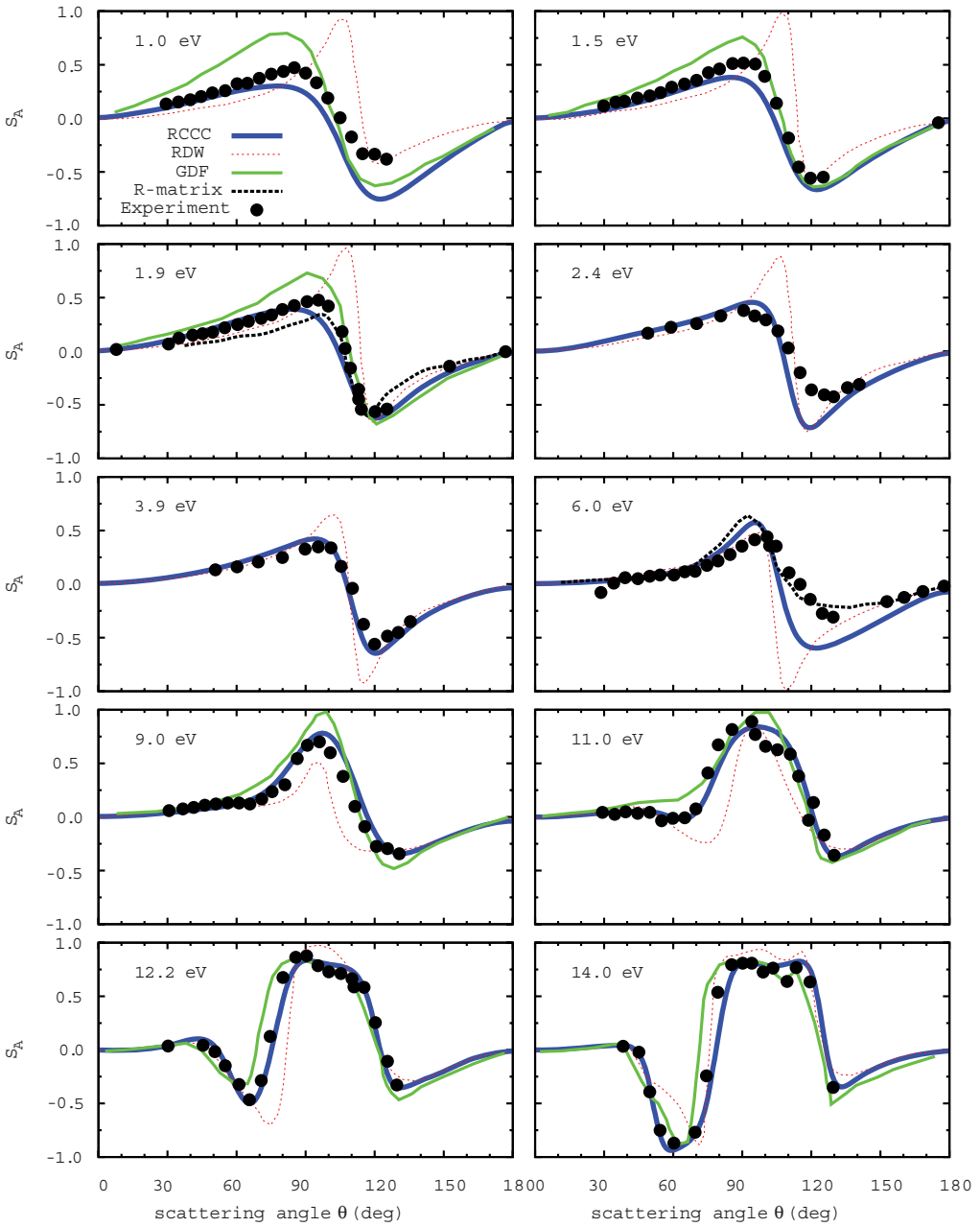


FIG. 2. (Color online) Spin-asymmetry parameter $S_A$ for elastic electron scattering on mercury. Measurements of Dummler *et al*. [16] (1.0, 1.5, and 1.9 eV), Kaussen *et al*. [17] (6, 9, 11, 12.2, and 14 eV), and Duweke *et al*. [18] (2.4 and 3.9 eV) are presented. The RCCC calculations are described in the text. The relativistic distorted-wave calculations of Szmytkowski and Sienkiewicz [14], the generalized density-functional calculations of Fritsche *et al*. [19] and Haberland and Fritsche [20], and the *R*-matrix calculations of Bartschat *et al*. [21] are denoted RDW, GDF, and *R*-matrix, respectively.

*et al*. [1] highlight the discrepancy between experiment and theory for the $P_2$ Stokes parameter of zinc. At 11 eV there is significant disagreement between theory and experiment. It is in this energy region that $3d^{10}$ core excitation levels exist; these states cannot be modeled accurately with the RCCC method, which assumes a closed $3d^{10}$ core. The NIST lists core excited states $(3d^9 4s^2 4p)\,^3P_1^o$, $(3d^9 4s^2 4p)\,^3D_1^o$, and $(3d^9 4s^2 4p)\,^3P_1^o$ at 11.187, 11.804, and 11.877 eV, respectively. Napier *et al*. [33] have shown that experimental elastic differential cross sections are affected by negative-ion resonances associated with these core excited states. The present RCCC model does not incorporate $3d^9 \ldots$ excited states and therefore these resonances could be responsible for the current discrepancy between the RCCC spin-asymmetry results and experiment at 11 eV. At 14 eV the agreement between theory is once again good; however, the measured peak in the spin-asymmetry parameter is a little sharper than that produced by the RCCC calculations.

The accuracy of the RCCC method in the calculation of the $S_A$ parameter for $e$-Hg scattering is illustrated in Fig. 2. Here the spin-asymmetry parameter is calculated across a wide range of energies and compared with the measurements due to Dummler *et al*. [16] at 1, 1.5, and 1.9 eV; Kaussen *et al*. [17] at 6, 9, 11, 12.2, and 14 eV; and Duweke *et al*. [18] at 2.4 and 3.9 eV. The results are also compared with the following theories: the relativistic distorted-wave calculations of Szmytkowski and Sienkiewicz [14] (denoted RDW); the generalized density-functional calculations of Fritsche *et al*. [19] at 1.0, 1.5, and 1.9 eV and Haberland and Fritsche [20] at 6, 9, and 11 eV (denoted GDF); and $R$-matrix calculations of Bartschat *et al*. [21] at 1.9 and 6 eV. The detector has an angular resolution of 3.5° at all energies except at 2.4 and 3.9 eV, where it is 8.0°. The angular resolution is incorporated by convolution of the RCCC results. There is excellent agreement between RCCC results and experiment at 1, 1.5, 1.9, 3.9, 9, 11, 12.2, and 14 eV. At 2.4 and 6 eV there is excellent agreement between the RCCC spin-asymmetry results and experiment at all angles except in the minima regions near 120° where the RCCC results are lower than experiment. We note that the RCCC spin-asymmetry results for Hg at 9 eV are in excellent agreement with experiment despite the fact that $5d^9 \ldots$ core excited states are listed in the NIST tables in this region at 8.79 and 9.54 eV [28].

Calculations performed without the phenomenological one- and two-electron polarization potentials resulted in only a marginal change in the Sherman function results for both Hg and Zn. When the polarization potentials are set to zero the calculated corresponding static dipole polarizabilites are $46.0a_0^3$ and $38.7a_0^3$ for Hg and Zn, respectively. The Sherman function results, unlike the energy levels and oscillator strengths of the target, are insensitive to the phenomenological one- and two-electron polarization potentials employed.

## IV. CONCLUSION

We have calculated the Sherman function for $e$-Zn and $e$-Hg scattering across a wide range of scattering angles and energies using the RCCC theory within the model of two active electrons above a Dirac-Fock core. Three key features of the RCCC method are critical: (i) an *ab initio* treatment of spin via the Dirac equation, (ii) a unitary treatment of the scattering process, and (iii) correct antisymmetrization of the total wave function. There is excellent agreement between the RCCC results and experiment for the case of Hg across a wide range of energies and similarly there is excellent agreement between RCCC results and experiment for Zn across the range of energies where $3d^{10}$ core excitation levels do not appear. Explicit treatment of core excitations is a difficult task that is not undertaken in the present work. Meanwhile, it would be interesting to determine if the $R$-matrix method of Zatsarinny and Bartschat [34] that has the capacity to directly account for core excitations would reproduce results in agreement with the experimental Zn Sherman function at 11 eV. We remain convinced that geometric phases are not required in *ab initio* relativistic scattering theories based on the Dirac equation.

## ACKNOWLEDGMENTS

Support from the Australian Research Council and Curtin University is acknowledged. We are grateful for access to the Australian National Computational Infrastructure and its Western Australian node iVEC.

[1] L. Pravica, J. F. Williams, D. Cvejanovic, S. Samarin, K. Bartschat, O. Zatsarinny, A. D. Stauffer, and R. Srivastava, Phys. Rev. A **83**, 040701 (2011).
[2] J. F. Williams, L. Pravica, and S. N. Samarin, Phys. Rev. A **85**, 022701 (2012).
[3] D. V. Fursa and I. Bray, Phys. Rev. Lett. **100**, 113201 (2008).
[4] C. J. Bostock, J. Phys. B **44**, 083001 (2011).
[5] C. J. Bostock, M. J. Berrington, D. V. Fursa, and I. Bray, Phys. Rev. Lett. **107**, 093202 (2011).
[6] M. J. Berrington, C. J. Bostock, D. V. Fursa, I. Bray, R. P. McEachran, and A. D. Stauffer, Phys. Rev. A **85**, 042708 (2012).
[7] J. Kessler, *Polarized Electrons* (Springer, Berlin, 1985).
[8] K. Bartschat, Phys. Rep. **180**, 1 (1989).
[9] N. Andersen and K. Bartschat, *Polarization, Alignment, and Orientation in Atomic Collisions* (Springer, Berlin, 2000).
[10] T. J. Gay, Adv. At. Mol. Phys. **57**, 157 (2009).
[11] P. G. Burke and J. F. B. Mitchell, J. Phys. B **7**, 214 (1974).
[12] M. Bartsch, H. Geesmann, G. F. Hanne, and J. Kessler, J. Phys. B **25**, 1511 (1992).
[13] R. P. McEachran and A. D. Stauffer, J. Phys. B **25**, 1527 (1992).
[14] R. Szmytkowski and J. E. Sienkiewicz, J. Phys. B **27**, 555 (1994).
[15] P. Kumar, A. K. Jain, A. N. Tripathi, and S. N. Nahar, Phys. Rev. A **49**, 899 (1994).
[16] M. Dummler, M. Bartsch, H. Geesmann, G. F. Hanne, and J. Kessler, J. Phys. B **25**, 4281 (1992).

[17] F. Kaussen, H. Geesmann, G. F. Hanne, and J. Kessler, J. Phys. B **20**, 151 (1987).
[18] M. Duweke, N. Kirchner, E. Reichert, and S. Schon, J. Phys. B **9**, 1915 (1976).
[19] L. Fritsche, C. Kroner, and T. Reinert, J. Phys. B **25**, 4287 (1992).
[20] R. Haberland and L. Fritsche, J. Phys. B **20**, 121 (1987).
[21] K. Bartschat, H. J. Goerss, and R. P. Nordbeck, Z. Phys. D **17**, 25 (1990).
[22] K. G. Dyall, I. P. Grant, C. T. Johnson, F. P. Parpia, and E. P. Plummer, Comput. Phys. Commun. **55**, 425 (1989).
[23] I. P. Grant and H. M. Quiney, Phys. Rev. A **62**, 022508 (2000).
[24] D. V. Fursa and I. Bray, J. Phys. B **30**, 5895 (1997).
[25] D. V. Fursa, I. Bray, and G. Lister, J. Phys. B **36**, 4255 (2003).
[26] A. Ye and G. Wang, Phys. Rev. A **78**, 014502 (2008).
[27] D. Goebel, U. Hohm, and G. Maroulis, Phys. Rev. A **54**, 1973 (1996).
[28] [http://physics.nist.gov/PhysRefData/ASD/levels_form.html].
[29] T. M. Miller and B. Bederson, Adv. At. Mol. Phys. **13**, 1 (1977).
[30] N. S. Scott, K. Bartschat, P. G. Burke, W. B. Eissner, and O. Nagy, J. Phys. B **17**, L191 (1984).
[31] N. Sherman, Phys. Rev. **103**, 1601 (1956).
[32] I. Bray, Z. Phys. D **30**, 99 (1994).
[33] S. A. Napier, D. Cvejanovic, P. D. Burrow, J. F. Williams, J. A. Michejda, and L. Pravica, Phys. Rev. A **80**, 042710 (2009).
[34] O. Zatsarinny and K. Bartschat, Phys. Rev. A **79**, 042713 (2009).